Energy Advances

ROYAL SOCIETY OF CHEMISTRY

COMMUNICATION

View Article Online
View Journal | View Issue

Cite this: *Energy Adv.*, 2025, 4, 387

Received 20th June 2024,
Accepted 30th January 2025

DOI: 10.1039/d4ya00390j

rsc.li/energy-advances

Contribution of organic carotenoid and carbonaceous biomass of *Tagetes erecta* flowers for enhanced solar hydrogen generation†

Sayantanu Mandal, Pawan Kumar and Kajari Kargupta *

Waste *Tagetes erecta* (Marigold) yellow-coloured flowers comprising carbonaceous biomass and organic pigment carotenoids are utilised for enhanced solar hydrogen generation through water splitting. The carbonaceous moiety of floral biomass, acting as a substrate is oxidised, makes uphill water splitting thermodynamically easier and improves the hydrogen production rate. Carotenoid, having visible light absorption and charge separation capability, acts as a photosensitizer when hybridised with semiconductors. A carotenoid–CdS nanohybrid photocatalyst exhibits an enhanced photocatalytic activity of 15 mmol g^{-1} h^{-1}, almost three times that of pristine CdS (5 mmol g^{-1} h^{-1}), when tested for hydrogen generation *via* water splitting under the full-band solar spectrum. The activity is further enhanced to 35 mmol g^{-1} h^{-1} (~7 times that of pristine CdS) when the *Tagetes erecta*–CdS photocatalytic system is used for water splitting. An AQE of ~17% is achieved using 420 nm of visible light.

The search for cleaner alternative energy sources for the world's growing needs has focused on hydrogen being able to replace traditional fossil fuels.[1] Among many technological advances capable of hydrogen generation, green hydrogen has drawn the attention of researchers and industries, as more organic/inorganic hybrid photocatalysts are being introduced.[2,3] Solar hydrogen generation *via* water splitting (without biomass) is achievable, but there are several bottlenecks, like thermodynamic barriers, photocorrosion, light conversion efficiency, low quantum yield and high recombination, which reduce the quantum efficiency and restrict commercialisation of the process.[4,5] Different research groups have been contributing to an enhancement in hydrogen generation *via* the addition of co-catalysts, carbon materials, 3D MOF hydrogels and quantum dots. However, very little research work has focused on the contribution of organic dyes from waste biomass to photocatalytic water splitting.[4,6–9] The inclusion of carbonaceous biomass along with water and sunlight (biomass reforming) reduces the thermodynamic barrier, provided the oxidation potential of biomass is more negative than the water oxidation potential.[10,11] The total process may be defined as the oxidation of electron-donating carbonaceous biomass and the splitting of water. While water splitting is an energy-consuming process, the oxidation of biomass is exergonic and exothermic. The combination of both processes may result in a slightly uphill reforming process.[10,11] A significantly higher rate of hydrogen production can be achieved by this process from a variety of feedstocks, which could be chosen from waste materials. Additionally, the organic dyes of coloured floral biomass, when hybridised with a semiconductor photocatalyst, act as photosensitizers. This kind of semiconductor-organic-pigment-based system has increased light-capturing capability and accelerated charge separation caused by two-step photoexcitation between the semiconductor photocatalyst and the dye.[12] To achieve modifying effects, the relationship between the LUMO level of the organic pigment and the photocatalytic activity was illustrated by Nagatomo *et al.*[9] Here, we report a novel bioconversion of yellow-coloured waste *Tagetes erecta* (TE) flowers, which have a high amount of organic carotenoid pigment, for enhanced solar hydrogen generation. The organic carotenoid pigment, comprising ~90% lutein and ~5% zeaxanthin,[13] acts with CdS as a nanohybrid photocatalyst for hydrogen generation; the carbonaceous biomass of floral waste acts as the substrate. Although there are a few reports available in the literature on biomass reforming utilizing different feedstocks, like wooden branches, sawdust, or rice husks,[10] there exists no report addressing the contribution of organic pigment as well as the carbonaceous part of biomass to boost solar hydrogen generation. Many efforts have been made to manage floral waste, like composting and bioconversion to dye or biodegradable materials, but utilizing floral waste in photocatalytic hydrogen generation is very valuable for the prospect of commercialization.[14,15] The waste *Tagetes erecta* (TE) is collected from religious institutions, events/ceremonies, households and commercial spaces. The waste *Tagetes erecta* has been pre-processed and converted into a fine

Chemical Engineering Department, Jadavpur University, Kolkata 700032, India. E-mail: karguptakajari2011@gmail.com

† Electronic supplementary information (ESI) available. See DOI: https://doi.org/10.1039/d4ya00390j

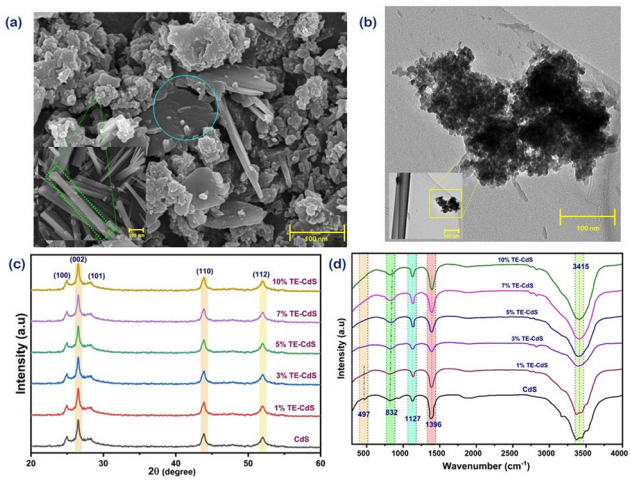

Fig. 1 FE-SEM micrograph images of (a) *Tagetes erecta*–CdS and CdS nanorod (inset). (b) TEM images of *Tagetes erecta*–CdS and CdS nanorod (inset). (c)) XRD analysis of CdS and various concentrations of *Tagetes erecta*–CdS. (d) FTIR analysis of CdS and various concentrations of *Tagetes erecta*–CdS.

powder *via* a freeze-drying method, followed by integration with semiconductor CdS to form *Tagetes erecta*–CdS (TE–CdS) nanohybrid (carotenoid-biomass–CdS) *via* a one-step hydrothermal method (Fig. S1, ESI†). To reveal the individual role of carotenoid (Car), it is extracted from *Tagetes erecta* powder followed by hybridization with CdS and used as a photocatalyst [carotenoid–CdS (Car–CdS)] for water splitting (without biomass). The homogeneously dispersed nanorod-like structure of CdS (82.07 nm) can be observed in the FE-SEM images (Fig. 1a). On the CdS nanorod, TE has been revealed to form an extra layer. TEM images confirm the nanorod-shaped CdS with an inter-planar distance of 0.34 nm for the (100) plane of CdS, and wrinkles in the surface due to thermal shrinkage of the carbon of TE (Fig. 1b). The EDX spectrum confirms the successful synthesis of the TE–CdS photocatalyst by the rise in individual peaks of Cd, S and C (Fig. S2a, ESI†). The zeta potential of the TE–CdS system reveals greater stability and lower chances of coagulation (−19.0 mV) (Fig. S3b, ESI†). The XRD peaks (Fig. 1c) show the different crystal planes that match the hexagonal wurtzite phase of CdS and correspond to the nanorod structure of CdS (JCPDS card no. 41-1049).[16] Due to the presence of the carbon moiety of TE–CdS, an increase in the crystallinity of CdS has been observed in the (100), (002), (101), (110) and (112) peaks corresponding to observations at 2θ of 25.11°, 25.92°, 28.46°, 43.59° and 51.48°. The intensities of the CdS-attributed peaks (100), (002), (110) and (112) increase due to the addition of TE, showing an increase in crystallinity. The FTIR spectra (Fig. 1d) reveal the Cd–S stretching band (596 cm^{-1}) and water bending vibrations (1625 and 3417 cm^{-1}).[17,18] The peak at 1056 cm^{-1} corresponds to the C–O bonds, and due to steric hindrance caused by C on Cd–S bonds, the peak at 596 cm^{-1} decreases as the carbon weight percentage (wt% of *Tagetes erecta*) increases.[19]

The XPS (Fig. S4 and S5, ESI†) analysis shows the interaction of CdS with TE, which is consistent with the FTIR results; it exhibits a number of oxygen-containing functional groups on the photocatalytic surface, including C–O and –OH, which might serve as traps to encourage charge separation.[20] TGA (Fig. S2c, ESI†) also confirms the integration of the carbon moiety of TE and CdS, as 44.3% mass loss is observed within the temperature range of 530 °C. The specific surface area (evaluated from BET analysis (Fig. S2d, ESI†) of mesoporous TE–CdS (26.9 $m^2\ g^{-1}$) is much higher than that of pristine CdS (18.6 $m^2\ g^{-1}$), resulting in more active sites for reduction–oxidation reactions. Larger pores are assumed to have developed following the aggregation of CdS crystals of different sizes, while smaller holes are assumed to be formed during crystal growth. The UV-vis spectra (Fig. 2a) show that TE–CdS nanohybrids have strong absorption in the range of visible light, and a redshifted absorption curve is obtained compared to pristine CdS, showing the improved light capturing ability of TE–CdS. This corresponds to a 2.32 eV band gap (less than the 2.43 eV band gap of pristine CdS), as obtained from the Tauc plot (Fig. S6, ESI†). This observation may be explained by the presence of TE-caused defect states and their impact on size control during nanoparticle formation.[21] The absorption spectrum of Car–CdS is intermediate between those of CdS and TE–CdS. It is revealed that the increase in the amount of TE in the photocatalytic system helps boost the photocatalytic activity. Photoluminescence spectra (Fig. 2b) reveal that the peak intensity of Car–CdS is lower than that of pristine CdS, indicative of lower recombination, *i.e.* segregation of photoexcited electrons and holes due to the presence of sensitizer dye. TE–CdS displays further decay in peak intensity value, indicating that the presence of biomass plays a role in lowering the recombination of electron–hole pairs. The addition of CdS to TE causes a redshift in the PL spectra, indicating molecular conjugation between CdS and *Tagetes erecta*, as also confirmed by the FTIR spectra.

TE–CdS (or its electrically conductive carbon surface) exhibits lower charge transfer resistance, as shown by the smaller arc radius of the Nyquist plot using EIS (Fig. 2c). Reduced charge resistance at solid–solid links (based on *Tagetes erecta*) signifies improved electron transfer. A cyclic voltammetry

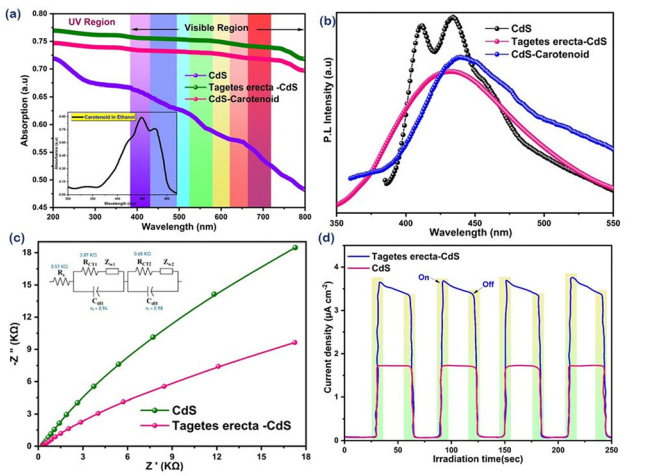

Fig. 2 (a) UV-vis spectra of CdS and *Tagetes erecta*–CdS. (b) Photoluminescence spectra. (c) EIS spectra of CdS and *Tagetes erecta*–CdS. (d) Transient photocurrent of pure CdS and *Tagetes erecta*–CdS under simulated light.

(Fig. S7, ESI†) study reveals an almost four times increase (compared to CdS) in current density, corresponding to onset and offset potential at 80 mV s^{-1} source rate; this implies faster electron transfer kinetics at the surface of the electrode. TE–CdS exhibits a higher transient photocurrent response than pristine CdS when exposed to an on/off sequence of visible light irradiation (Fig. 2d); this implies a higher absorption rate of photons, an enhancement in mobility and better charge transport. The hybrid photocatalytic systems (TE–CdS and Car–CdS) along with water were subjected to solar irradiation for 6 h for hydrogen generation. A solar simulator (Newport Oriel LCS-100) with an air mass filter (AM 1.5 G) was used to obtain one solar sun intensity (113 mW cm^{-2}). In all cases, 50 mg of photocatalyst was uniformly dispersed in 25 mL of water and Na_2S was used as a sacrificial agent; no hydrogen generation was observed before solar irradiation. A remarkable enhancement (~7 times) in photocatalytic activity (mmol H_2 generated h^{-1} $g_{cat}{}^{-1}$ over a period of 6 h) was observed using the TE–CdS photocatalytic system (with varying composition of 1–10 wt% of *Tagetes erecta*) in place of pristine CdS (Fig. 3a). The best performance was achieved at an optimum 5% composition of *Tagetes erecta*; beyond the optimum, the activity decayed slightly due to an increase in the amount of carbon surface, which shades the CdS nanorod. Fig. 3b and c compare the cumulative hydrogen evolution (mmol) and photocatalytic activity, respectively, for different photocatalytic systems, *viz.* 5% TE–CdS, Car–CdS and pristine CdS.

The Car–CdS photocatalyst enhances hydrogen evolution through water splitting (in the absence of carbonaceous biomass) due to photosensitization of carotenoid and exhibits almost 3 times higher photocatalytic activity than pristine CdS (~15 mmol h^{-1} g^{-1}). The TE–CdS (carotenoid–carbonaceous biomass–CdS) system generates hydrogen almost linearly, with irradiation time, with an average hydrogen evolution rate of ~1.88 mmol h^{-1} and photocatalytic activity of ~35 mmol h^{-1} g^{-1} (~7 times enhancement w.r.t. CdS and ~2.3 times w.r.t. Car–CdS) in the full-band spectrum, indicating the significant role of carbonaceous biomass in water splitting. A slight (<18%) reduction in evolution rate and activity (~30 mmol h^{-1} g^{-1}) and an apparent quantum efficiency of 17.25% are obtained using a 420 nm band pass filter. The results reveal that the TE–CdS photocatalytic system is mostly visible light active, as the carotenoid absorbs generally blue, green and violet visible light from the solar spectrum. The performance of the photocatalyst was also checked with a variation in different solar intensities (100–300 mW cm^{-2}). It was found that with an increase in solar intensity, the hydrogen evolution also increases (Fig. S8, ESI†). Four successive cycles were used to assess photocatalyst recyclability. The TE–CdS loses around 18% and Car–CdS loses around 19.2% of its original activity by day 30 after 4 cycles (Fig. 3d and Table S2, ESI†). Following the reaction, only a small amount of metal loss is seen as a consequence of photocorrosion, which happens when S^{2-} oxidizes after being exposed to photogenerated holes for an extended period, leading to photocatalyst failure.[22] After the 4 cycles, no change in the morphology was seen and the decrease in photocatalytic hydrogen generation is due to the elution and decomposition of carotenoid pigments from TE–CdS, as confirmed by the decrease in the absorption peaks (Fig. S9a and b, ESI†). A cell viability test shows high viability percentage in Car–CdS and TE–CdS (47.1%) compared to pristine CdS (9.8%) after 72 h (Fig. S10, ESI†). The carotenoid moiety helps to prevent oxidative damage to the cellular structure by scavenging free radicals, reducing the risk of cell damage.

Fig. 4 shows the probable two-step excitation and charge transfer mechanism in TE–CdS containing organic carotenoid pigment. The carotenoid moiety has long organic chains, and the energy of the excited singlet state tends to be consumed in molecular motion and it is easy to convert the excited energy into water splitting to generate hydrogen, as the carotenoid moiety also performs as a charge separator.[9] During solar irradiation, the carotenoid moiety of *Tagetes erecta* (the chromophore) absorbs visible light and is stimulated from its ground state to its excited state. CdS absorbs light and creates

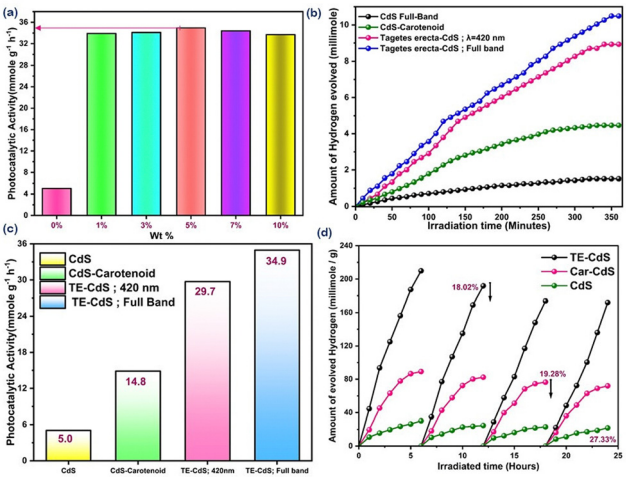

Fig. 3 (a) Cumulative hydrogen generation for different ratios of *Tagetes erecta*–CdS. (b) Cumulative hydrogen generation *versus* irradiation time for of CdS and *Tagetes erecta*–CdS using the full-band solar spectrum and 420 nm wavelength. (c) Photocatalytic activity. (d) Recyclability analysis.

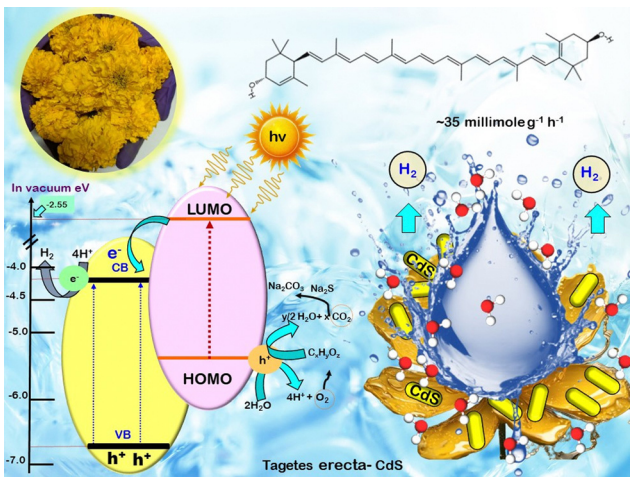

Fig. 4 Photogenerated charge separation phenomena and the proposed photocatalytic process.

electron–hole pairs. Electrons move from the valence band to the conduction band of CdS:

$$\text{Car–CdS} + h\nu \rightarrow \text{Car}^{*}\text{–CdS}[(h^{+}) + (e^{-})] \quad (1)$$

A photoelectron generated by the excited chromophore is driven from LUMO of carotenoid straight into the conduction band (CB) of the semiconductor CdS and an associated carotenoid radical cation is generated; the carotenoid radical cation is reduced by the electron-donating sacrificial agent (SED, Na_2S) to regenerate the ground-state carotenoid:

$$\text{Car}^{*}\text{–CdS}((h^{+}) + (e^{-})) \rightarrow \text{Car}^{*+}\text{–CdS}(e^{-}) \quad (2)$$

$$\text{Car}^{*+}\text{–CdS}(e^{-}) + \text{SED} \rightarrow \text{Car–CdS}(e^{-}) + \text{SED}^{+} \quad (3)$$

Oxidation of water generates a proton (OER):

$$2\text{Car}^{+} + 2H_2O \rightarrow \frac{1}{2}O_2 + 2H^{+} \quad (E_O = 1.23\ \text{eV}). \quad (4)$$

The electrons in the CB of semiconductor CdS are utilized in hydrogen generation (HER) *via* proton reduction:

$$2H^{+} + 2e^{-} \rightarrow H_2\ (\text{CB of CdS};\quad E_O = 0\ \text{eV}) \quad (5)$$

The photocatalytic performance of CdS–carotenoid is thus enhanced by two-step excitation, increased absorption of visible light, effective charge separation between CdS and the carotenoid moiety, increased electron mobility, and reduced recombination by preventing the delivered electron from recombining with the hole caused by separating cations on the carotenoid moiety. Furthermore, the presence of electron-donating carbonaceous biomass promotes electron transfer and it is oxidized, utilizing the enhanced oxygen produced due to presence of carotenoid:[23]

$$C_xH_yO_z + \left(x + \frac{y}{4} - \frac{z}{2}\right)O_2 \rightarrow \frac{y}{2}H_2O + xCO_2 \quad (\Delta G_0\ \&\ \Delta H_0 < 0) \quad (6)$$

Oxidation of the electron-donating carbonaceous part of the floral biomass, along with water splitting, facilitates enhanced hydrogen production *via* the overall reaction:

$$C_xH_yO_z + (2x - z)H_2O \rightarrow (2x + y/2 - z)H_2 + xCO_2 \quad (7)$$

Sacrificial agent Na_2S leads to the evolution of hydrogen and chemically absorbs CO_2:[24]

$$Na_2S + CO_2 + H_2O \rightarrow Na_2CO_3 + H_2S \quad (8)$$

In summary, a thorough analysis was carried out on recyclable, environmentally stable TE–CdS for increased solar hydrogen production by photocatalytic water splitting under the full-band spectrum of simulated light, using Na_2S as a sacrificial agent. The carotenoid-sensitized *Tagetes erecta*–CdS exhibits remarkable enhancement in solar hydrogen generation in comparison with other reported dye-sensitized systems (Table S5, ESI†) or other photocatalytic systems with different substrates (Table S6, ESI†). The dual presence of carotenoid and electron-donating carbonaceous biomass stabilizes the photocatalytic system in the full-band solar spectrum, minimizes photocorrosion, improves photoresponse, light absorption and charge transfer, promotes the separation of photogenerated hole–electron pairs (confirmed using PL and UV-Vis spectra), reduces the thermodynamic barrier and enhances hydrogen generation (35 mmol g^{-1} h^{-1}; AQE: 17.25%). The cost analysis tabulated in Table S4 (ESI†) reveals a 50% reduction in normalized cost (with hydrogen production rate) of TE–CdS compared to pristine CdS. This novel utilization of waste *Tagetes erecta* in enhanced hydrogen generation is significant in the context of energy applications, carbon recycling and remedying environmental pollution.

Data availability

The author confirms that the data supporting the findings of the study are available within the article and ESI.† Raw data that supports the finding of the study are available from the corresponding author, upon reasonable request.

Conflicts of interest

There are no conflicts to declare.

Notes and references

1 Y. Li, Y. Liu, T. Zheng, A. Li, G. G. Levchenko, W. Han, A. V. Pashchenko, S. Sasaki, H. Tamiaki and X.-F. Wang, *Green Chem.*, 2024, **26**, 1511–1522.
2 T. Mazuelo, T. Naranjo, M. Gomez-Mendoza, A. Herrero Pizarro, L. Collado, M. Barawi, F. Gándara, M. Liras and V. A. De la Peña O'Shea, *J. Mater. Chem. A*, 2024, **12**, 1476–1487.
3 A. Sarkar, A. Mandal, S. Mandal, S. K. Sen, D. Banerjee, S. Ganguly and K. Kargupta, *J. Chem. Sci.*, 2024, **136**, 2.
4 A. Naldoni, M. Altomare, G. Zoppellaro, N. Liu, Š. Kment, R. Zbořil and P. Schmuki, *ACS Catal.*, 2018, **9**, 345–364.
5 S. Ragab, M. R. Elkatory, M. A. Hassaan and A. El Nemr, *Sci. Rep.*, 2024, **14**, 1019.
6 S. Mandal, A. Sarkar, P. Mukherjee, S. Das, D. Banerjee, S. Ganguly and K. Kargupta, *Int. J. Hydrogen Energy*, 2024, **51**, 1167–1185.
7 F. Li, J. Yang, J. Gao, Y. Liu and Y. Gong, *Int. J. Hydrogen Energy*, 2020, **45**, 1969–1980.
8 Z. Jiang, X. Zhang, G. Yang, Z. Yuan, X. Ji, F. Kong, B. Huang, D. D. Dionysiou and J. Chen, *Chem. Eng. J.*, 2019, **373**, 814–820.
9 M. Nagatomo, H. Hagiwara, S. Ida and T. Ishihara, *Electrochemistry*, 2011, **79**, 779–782.
10 K. A. Davis, S. Yoo, E. W. Shuler, B. D. Sherman, S. Lee and G. Leem, *Nano Convergence*, 2021, **8**, 6.
11 H. Luo, J. Barrio, N. Sunny, A. Li, L. Steier, N. Shah, I. E. Stephens and M. Titirici, *Adv. Energy Mater.*, 2021, **11**, 2101180.
12 Y. Liu, Y. Li, G. Chen, X. Wang, R. Fujii, Y. Yamano, O. Kitao, T. Nakamura and S. Sasaki, *Adv. Mater. Interfaces*, 2021, **8**, 2101303.
13 L. Fernandes, E. Ramalhosa, J. Pereira, J. Saraiva and S. Casal, *Agriculture*, 2018, **8**, 146.

14 G. Elango and R. Govindasamy, *Environ. Sci. Pollut. Res.*, 2018, **25**, 10688–10700.
15 P. Singh, R. Singh, A. Borthakur, S. Madhav, V. K. Singh, D. Tiwary, V. C. Srivastava and P. K. Mishra, *Waste Manage.*, 2018, **77**, 78–86.
16 A. Sarkar, M. K. Mandal, S. Das, S. Mandal, P. Chakraborty, A. Mandal, D. Banerjee, S. Ganguly and K. Kargupta, *Opt. Mater.*, 2024, **147**, 114670.
17 Q. Li, B. Guo, J. Yu, J. Ran, B. Zhang, H. Yan and J. R. Gong, *J. Am. Chem. Soc.*, 2011, **133**, 10878–10884.
18 L. Ge, F. Zuo, J. Liu, Q. Ma, C. Wang, D. Sun, L. Bartels and P. Feng, *J. Phys. Chem. C*, 2012, **116**, 13708–13714.
19 Ch. V. Reddy, J. Shim and M. Cho, *J. Phys. Chem. Solids*, 2017, **103**, 209–217.
20 P. Wang, J. Zhang, H. He, X. Xu and Y. Jin, *Nanoscale*, 2015, **7**, 5767–5775.
21 J.-Q. Chang, Y. Zhong, C.-H. Hu, J.-L. Luo and P.-G. Wang, *J. Mol. Struct.*, 2019, **1183**, 209–216.
22 R. Peng, D. Zhao, J. Baltrusaitis, C.-M. Wu and R. T. Koodali, *RSC Adv.*, 2012, **2**, 5754.
23 S. N. Jaafar, L. J. Minggu, K. Arifin, M. B. Kassim and W. R. Wan, *Renewable Sustainable Energy Rev.*, 2017, **78**, 698–709.
24 V. Kumaravel, M. Imam, A. Badreldin, R. Chava, J. Do, M. Kang and A. Abdel-Wahab, *Catalysts*, 2019, **9**, 276.